



Original Article

Finite Element Model of a Deformable American Football Helmet Under Impact

J. SEBASTIAN GIUDICE ¹, ADRIAN CAUDILLO,¹ SAYAK MUKHERJEE,¹ KEVIN KONG,¹ GWANSIK PARK,²
RICHARD KENT,^{1,2} and MATTHEW B. PANZER¹

¹Center for Applied Biomechanics, Department of Mechanical and Aerospace Engineering, University of Virginia, 4040 Lewis and Clark Dr., Charlottesville, VA 229011, USA; and ²Biomechanics Consulting and Research (Biocore), LLC, Charlottesville, VA, USA

(Received 10 November 2019; accepted 29 January 2020; published online 7 February 2020)

Associate Editor Joel Stitzel oversaw the review of this article.

Abstract—Despite the use of helmets in American football, brain injuries are still prevalent. To reduce the burden of these injuries, novel impact mitigation systems are needed. The Vicis Zero1 (VZ1) American football helmet is unique in its use of multi-directional buckling structures sandwiched between a deformable outer shell and a stiff inner shell. The objective of this study was to develop a model of the VZ1 and to assess this unique characteristic for its role in mitigating head kinematics. The VZ1 model was developed using a bottom-up framework that emphasized material testing, constitutive model calibration, and component-level validation. Over 50 experimental tests were simulated to validate the VZ1 model. CORrelation and Analysis (CORA) was used to quantify the similarity between experimental and model head kinematics, neck forces, and impactor accelerations and forces. The VZ1 model demonstrated good correlation with an overall mean CORA score of 0.86. A parametric analysis on helmet compliance revealed that the outer shell and column stiffness influenced translational head kinematics more than rotational. For the material parameters investigated, head linear acceleration ranged from 80 to 220 g, whereas angular velocity ranged from 37 to 40 rad/s. This helmet model is open-source and serves as an *in silico* design platform for helmet innovation.

Keywords—American football, Safety, Research and development, Parametric investigation, Concussion.

INTRODUCTION

It is estimated that 1.6–3.8 million sports-related traumatic brain injuries (TBIs) occur annually in the United States.¹⁸ In American football (henceforth, football), players wear helmets that are designed to reduce the energy transferred to the head during an impact. The majority of modern helmets consist of a stiff outer shell, padding components, a facemask, and a chinstrap. In most helmets, the primary energy dissipation mode is through the compression and shearing of these padding elements.^{17,19} While modern football helmets are effective in reducing the incidence of severe head injuries (e.g. skull fracture), concussion remains a significant burden on the athletic population.^{9,19}

Using a different approach to helmet design, the Vicis Zero1 (VZ1, Vicis, Inc., Seattle, WA) helmet features a compliant outer shell and an internal columnar structure that locally deforms and buckles upon impact.²⁴ The VZ1 also includes a padding bonnet consisting of viscoelastic materials intended to provide additional energy dissipation. In the 2017 helmet assessment program used by the National Football League (NFL),⁵ to assess a helmet's ability to mitigate translational and rotational head kinematics, the VZ1 helmet was ranked as the top performer.²⁰

Computational modeling techniques have been crucial for the development of impact mitigation structures in the automotive and other industries, but finite element (FE) models have not historically played an important role in the development of football helmets. However, in 2018 the NFL funded the “Engineering Roadmap”, which included the development of open-source FE models of four modern football

Address correspondence to Matthew B. Panzer, Center for Applied Biomechanics, Department of Mechanical and Aerospace Engineering, University of Virginia, 4040 Lewis and Clark Dr., Charlottesville, VA 229011, USA. Electronic mail: panzer@virginia.edu

helmets, including the VZ1, and the associated impact assessment conditions to provide tools for the efficient analysis of helmet design, and facilitate the investigation of helmet mechanics as they relate to fundamental injury biomechanics.²¹ Through this program, models were developed using a comprehensive bottom-up approach that focuses on material testing, constitutive model calibration, and component-level validation.^{2-4,11}

As part of the same program, this study developed and validated an open-source FE model of the VZ1 helmet to simulate the impact conditions commonly used in helmet test and evaluation programs. The helmet model was validated in four separate impact configurations that utilized both the Hybrid-III head-neck (HIII H-N),²² and the National Operating Committee on Standards for Athletic Equipment headform (NOCSAE,¹⁵). However, the objective of this study was to perform an exploratory parametric analysis on the properties of the VZ1 helmet that make it unique, principally the compliance of the outer shell and the stiffness of the buckling columns, and investigate how these components affect the resulting head kinematics during helmet impact. This work should provide insight into the methods and strategies that will help improve future helmet design.

METHODS

The helmet model development process included medical imaging and segmentation to obtain component geometries, numerical implementation, material characterization and calibration, positioning and fitting the helmet to HIII H-N and NOCSAE headforms, comprehensive validation at the component level and in full-scale impact simulations, and a preliminary investigation on the role of effective helmet stiffness on mitigating head kinematics. These phases are described in the following sections and summarized in Fig. 1.

Helmet Model Geometry

The VZ1 helmet (Safety Equipment Institute Model Number 01; Fig. 2) consists of 450 polymeric columns sandwiched between two thin polymeric sheets (1.4–2.0 mm). The columns are adhered to the deformable external helmet shell (variable thickness), and to a stiff internal shell (2 mm thick). Attached to the internal shell is a padding bonnet that is made up of 19 individual pads which contact the head. Each padding component is composed of two layers of different viscoelastic foam materials and is contained within a

thin fabric layer. Five additional padding components provide further support to the forehead and jaw.

Model geometry was obtained using a series of computed tomography (CT) scans of the VZ1 helmet (Size A). Scans were obtained with the helmet fully assembled, fully disassembled, and fully assembled and fit with a 3D-printed NOCSAE headform. To maximize image quality, the facemask and all other metal components were removed. Each individual helmet component was segmented from the helmet scans using a combination of predefined segmentation thresholds and manual correction. All segmentation was performed using Mimics software (v21, Materialise, Leuven, Belgium). The facemask and chinstrap were scanned separately using a commercially available handheld 3D scanner (Artec Eva, Artec3D, Luxembourg) and processed similarly to the CT images.

Model Implementation

An FE model of the helmet was developed for LS-DYNA (Livermore Software Technologies Corporation, LSTC). Thin structures (e.g. external and internal shells) were meshed using 2D quadrilateral elements. Except for the outer helmet shell, the thicknesses of all thin structures were measured and assigned uniformly to the shell elements of the respective parts. Variable thickness of the external shell was measured from the CT scans and assigned at nodal resolution. All padding components were meshed using 3D hexahedral elements. The facemask and buckling columns were meshed using 1D beam elements located at the midline of the cylindrical geometry. To capture the correct buckling mode (approximately a fixed–fixed boundary condition), each buckling column required 16 elements along its buckling length as determined by a preliminary convergence study (see Supplementary Material). To enforce the fixed–fixed boundary condition, a beam element support structure was implemented on either end of each buckling column. This support structure was composed of an intermediate beam element, which connected the buckling column to the column shell part, and four support columns which constrained the end buckling column element and intermediate beam element to the surrounding column shell nodes. Therefore, each individual buckling column required 26 beam elements—16 elements within the buckling length of the column (shown in Black in Fig. 3), 2 intermediate elements (shown in yellow in Fig. 3), and 8 support elements (shown in green in Fig. 3). Through this implementation, the buckling length of each element was composed of 16 elements and the fixed–fixed boundary condition was maintained. This approach was required as nodes belonging to shell elements do

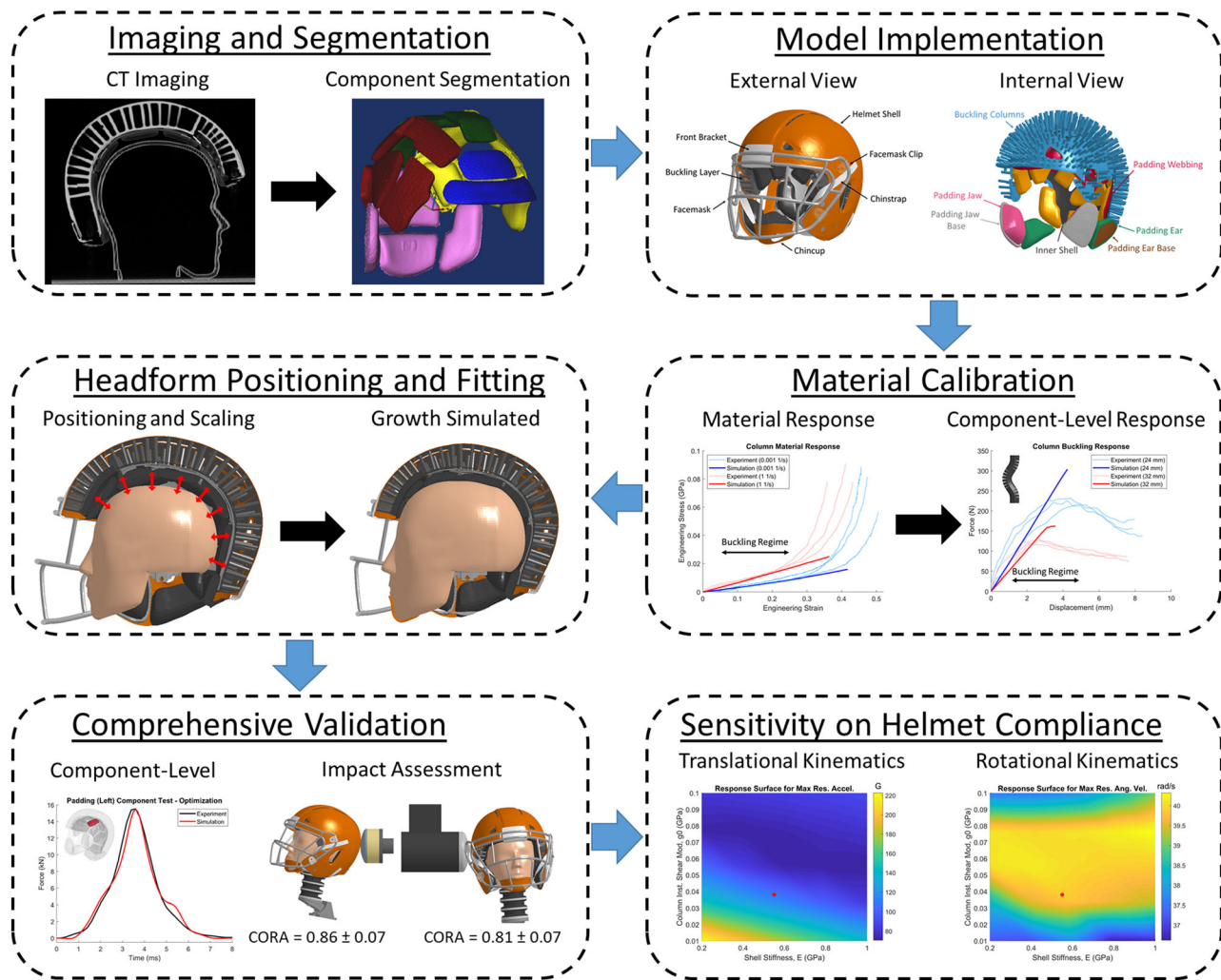


FIGURE 1. Summary of the Vicis Zero1 helmet model development process.

not resist nodal rotations¹³ and was verified using single column buckling simulations.

The masses of each helmet component were measured separately and used to define the densities of each model part. In total, the helmet model weighed 2.23 kg and was composed of 125,000 nodes, 128,000 elements, and 58 parts. Details regarding the mesh characteristics, mesh quality, and mass and inertia properties are included in the Supplementary Materials.

In the physical helmet, many of the structural components were rigidly connected through an adhesive epoxy. In the model, the corresponding parts were constrained through a tied contact (*CONTACT_TIED_SURFACE_TO_SURFACE_OFFSET, in LS-DYNA).¹⁴ Single surface contacts (*CONTACT_AUTOMATIC_SINGLE_SURFACE and *CONTACT_AUTOMATIC_GENERAL, in LS-DYNA) were included to define self-contacts between the numerous

helmet parts, including the buckling columns. In the physical helmet, snap fasteners were used to connect several of the padding and chinstrap components to the outer shell. In the model, these were represented using constrained nodal rigid bodies (*CONSTRAINED_NODAL_RIGID_BODIES, in LS-DYNA). Finally, four revolute joints were defined to constrain the facemask beams to the facemask clips (*CONSTRAINED_JOINT_REVOLUTE, in LS-DYNA).

Material Characterization and Calibration

A total of 23 experimental tests were conducted to characterize the 15 different materials found in the VZ1 helmet. Small material specimens were extracted from the helmet and loaded in compression and/or tension over a range of quasi-static (10^{-3} 1/s) to intermediate rates (10^0 1/s). These material tests are summarized in the Supplementary Materials. Materials specimens

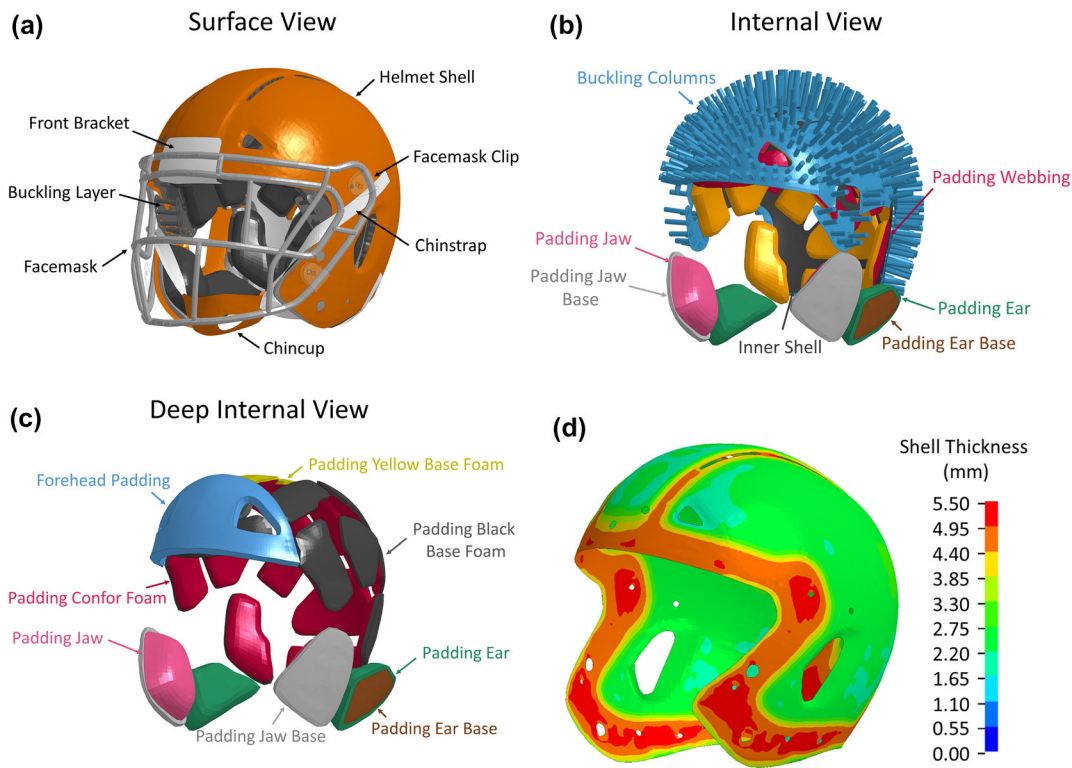


FIGURE 2. Overview of the VZ1 helmet: (a) surface view; (b) internal view highlighting the buckling column layer; (c) deep internal view highlighting padding components (the fabric layer that encapsulates the foam is not shown); and (d) variable shell thickness of the outer helmet shell.

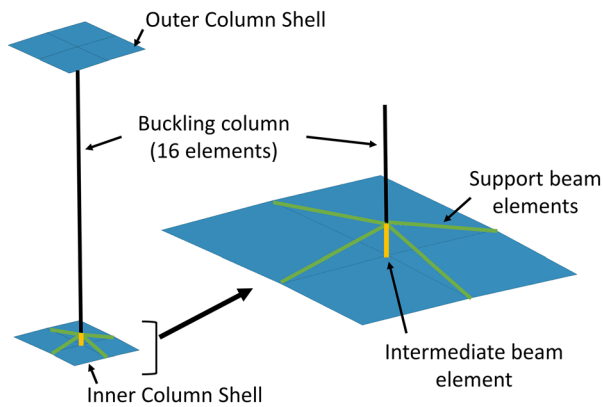


FIGURE 3. Schematic of the buckling column implementation. Support columns were generated on the inner and outer ends of the columns to enforce the fixed-fixed boundary condition. The use of 16 beam elements between the support columns was required to capture the correct buckling mode.

were extracted from the padding foams, padding liners, inner and outer shells, buckling columns, brackets, and chinstrap. Low rate (10^{-3} – 10^{-1} 1/s) and low force (< 200 N) material tests were conducted using a Bose Electroforce Test Bench (TA Instruments, New Castle, DE) configured for either compression or tension

loading modes. High force (> 200 N) and low rate (10^{-3} – 10^{-1} 1/s) material tests were conducted using an Instron Model 8874 test device (Instron, Canton, MA) configured for either compression or tension loading modes. At least three different samples were tested for each strain rate.

The outer and inner shells, brackets, jaw pad bases, facemask, and chinstrap were modeled using a linear elastic constitutive model with a Young's modulus determined from the respective material test data. A Kelvin representation of a linear viscoelastic material response (*MAT_VISCOELASTIC, in LS-DYNA). For this constitutive model, the shear relaxation function was dependent on the long (G_{∞}) and short-term (G_0) shear moduli, and a single time constant (β). A single beam element model with the exact dimensions of one of the tested specimens was simulated to calibrate G_{∞} , G_0 , and β , using the boundary conditions from the quasi-static (10^{-3} 1/s) and intermediate rate (10^0 1/s) material tests. In this study, all material models were calibrated using a conjugate-gradient algorithm, which was implemented through a custom Matlab script (R2017a, The Mathworks, Inc., Natick, MA, USA). A non-linear viscous foam constitutive model (*MAT_LOW_DENSITY_VISCOUS_FOAM,

in LS-DYNA) was used to model the padding foams. This material card used linear viscoelasticity to calculate the rate-dependent response based on a predefined quasi-static stress–strain curve. For each of these materials, the quasi-static stress–strain curve was obtained directly from quasi-static material tests (10^{-1} 1/s). The intermediate rate material test (10^0 1/s) data was used to tune the longer-term viscoelastic time constants ($\beta = 0.1, 0.01, 0.001$ 1/ms) using a single element simulation with the same dimensions as one of the tested specimens. Finally, a fabric-specific constitutive model (*MAT_FABRIC, in LS-DYNA) was used to model the padding webbing that covered the base of the padding foam, as well as the fabric that coated the outer surface that interacts with the headform. In these materials, experimentally measured stress–strain curves defined the loading and unloading response of the fabric in the normal and shear directions. Further information regarding these material models can be found in the LS-DYNA user manuals.¹⁴

Component-Level Validation

Twelve component-level simulations were performed to validate the material models. The assessed components included the inner and outer shells, face-mask, padding components, and buckling columns. The padding component tests were performed using a custom-built drop tower with an impact velocity of 5 m/s. These dynamic impact tests yielded strain rates on the order of 10^2 1/s. A summary of the component-level validation process is provided in the Supplementary Materials. For the padding materials, the dynamic component-level simulations were used to calibrate the short-term viscoelastic time constants ($\beta = 10, 1$ 1/ms). For this process, the component-level data for one of the padding components in the padding bonnet (19 components overall) was used to calibrate these short-term parameters and the data for 3 other padding components were used to verify the response. Furthermore, the response of the buckling column was verified by simulating the buckling of a single column with 16 elements along its length. Any material that was modified during the component-level validation stage was reassessed in the previous simulations used to obtain the material response, if applicable.

Helmet Fitting

A standardized fitting procedure (Fig. 4) was used to fit the helmet model onto FE models of the HIII H–N (v1.3 available at <http://biocorellc.com/finite-element-models/>) and NOCSAE (v1.0 available at <http://biocorellc.com/finite-element-models/>) headforms.^{3,4,11} First, the helmet model was positioned relative to the

headform. Helmet positioning was dictated by index points physically measured on the helmet and headform with the helmet positioned according to experimental protocols. For the NOCSAE headform, these points were measured from the CT scans of the VZ1 donned on a 3D printed NOCSAE headform. For the HIII headform, these index points were measured using a Romer arm. Using these target points, spatial rigid body transformations were generated to transform the nodal coordinates in the helmet model to the headform coordinate system. Once positioned, the headform model was scaled down by 30–50% such that the headform fit within the helmet space without penetrating the internal helmet components (Fig. 4). Next, a simulation was run to simulate the expansion of the shrunk headform to its original size. By enabling contact between the headform and the internal helmet components, the appropriate amount of pre-compression in the padding components was attained. Non-padding helmet parts (e.g. outer and internal shells, buckling layer) were fully constrained during the expansion simulation. The nodal coordinates of the compressed padding components were exported and used to create HIII- and NOCSAE-specific helmet models. Element quality and initial penetration checks were then performed, heavily distorted elements were re-meshed, and any initial penetrations were removed. Finally, the chinstrap was positioned.

Validation and Verification

A total of 62 simulations were simulated with the full helmet, using either a HIII H–N or NOCSAE headform model (Table 1). The HIII H–N was used to evaluate the helmet in pendulum (PI) and linear (LI) impact conditions. The primary difference between these two cases was that the LI case utilized a deformable impactor. The impactor deformation came from the compression of a vinyl nitrile (VN) foam puck sandwiched between the impact surface and ram. The pendulum used in the PI case was rigid. All simulations were run for 50 ms. In these impact simulations, helmet model performance was assessed by comparing the simulated head kinematics (linear acceleration, angular velocity) to the experimentally measured time histories. These metrics were chosen as they are currently used in the NFL’s helmet ranking system, which assesses helmet performance using the “Combined Metric”, a function of linear and angular head kinematics.⁵ Upper neck load cell (UNLC) force, and impactor acceleration were also compared to the equivalent experimental measures. In the LI condition, impactor force was also included in the comparison. Drop impacts were performed with both the HIII (DI-H) and NOCSAE (DI-N) headforms and the simulated

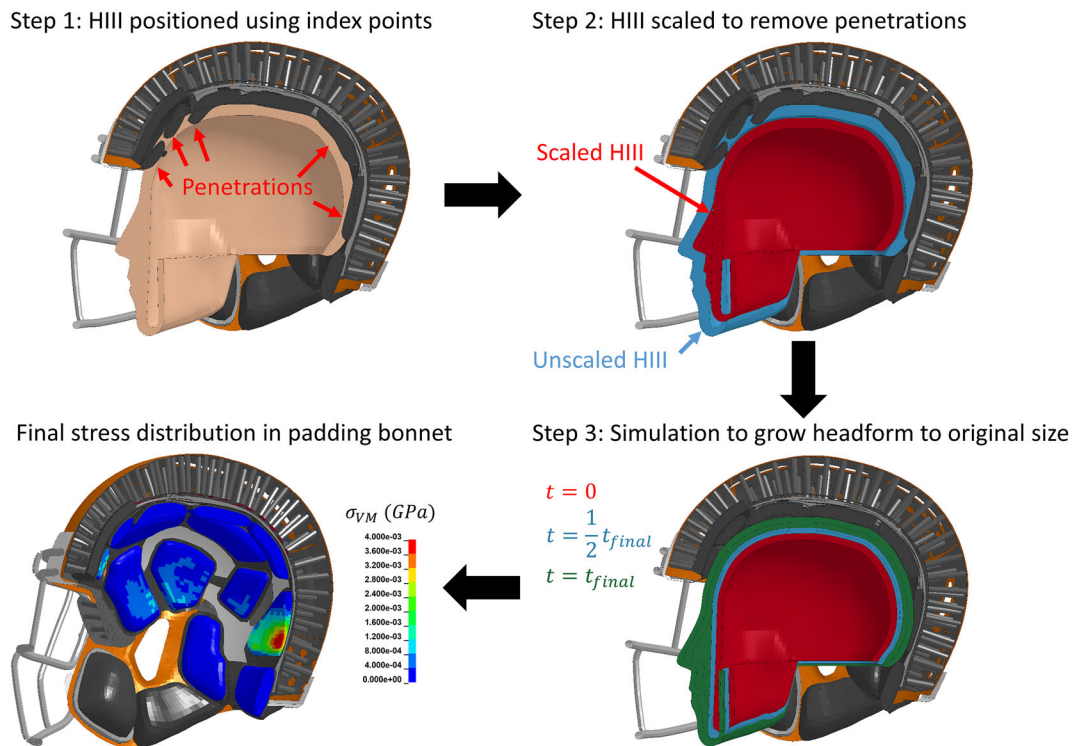


FIGURE 4. Overview of the helmet fitting process demonstrated with the HIII headform. Step 1: the HIII was positioned relative to the helmet using index points directly measured from the physical HIII and helmet. Step 2: the HIII was scaled down such that all penetrations between the scaled HIII and padding components were removed. Step 3: Growth of the HIII from the scaled size to the original size was simulated. Contact between the HIII and padding components allowed for the padding components to compress. Shown is the time progression from the scaled HIII at $t=0$ (red) to an intermediate state at $t=0.5t_{final}$ (blue) to the final state at $t=t_{final}$ (green). The final deformed padding components and Von-Mises stress (σ_{VM}) distribution in the padding bonnet is shown in the bottom left panel. The same process was used to fit the helmet model on the NOCSAE headform.

TABLE 1. Model validation simulation matrix.

Impact condition	Dummy model	Impact location	Impact velocity (m/s)	Number of simulations
PI	HIII H-N	Back, frontal ^a , FrontBoss, side	3.0; 4.6; 6.1	12
LI	HIII H-N	A, AP, B, C, D, F ^a , R, UT	5.5; 7.4; 9.3	24
DI-N	NOCSAE	Back, front, mask ^a , side, top	2.9; 4.9; 6.0 ^b	14
DI-H	HIII H-N	Back, front, side, top	2.9; 4.9; 6.0	12

^aRun for stability purposes only.

^bExperimental tests for the DI-N mask impact were not conducted and excluded.

head kinematics (linear acceleration) and load cell force were compared to experimental data. Further information regarding the dummy and impact condition simulations are available in Giudice *et al.*¹¹ The final simulation matrix included 24 LI, 12 PI, 14 DI-N, and 12 DI-H simulations. The PI and LI front impacts were run for stability purposes only and were not included in the model validation assessment. This was due to atypical helmet interactions that occurred between the helmet and impactor in the experimental tests.

Objective Rating

CORrelation and Analysis (CORA) scores⁸ were used to quantify the similarity between the model and experimental responses for head kinematics and neck kinetic outputs. In short, CORA uses a cross-correlation algorithm to assess similarities in phase, magnitude, and slope between two signals. Scores range from 0 to 1, where 0 indicates no similarity and a score of 1 indicates a perfect match between the two signals. For linear response histories (head acceleration, neck force, impactor acceleration, and impactor force), CORA was computed using the resultant response. For

angular metrics, a composite CORA (cCORA) score was computed using the method outlined in Giudice *et al.*¹¹ All CORA scores were computed over the first 30 ms of the simulation response, which captured peak head kinematics and neck kinetics in all cases. In all impact cases, the percent difference between experimental and simulation maximum resultant head linear acceleration and angular velocity were also computed.

Parametric Study on Helmet Stiffness

A parametric sensitivity study was performed to investigate the effect of helmet outer shell and buckling column stiffness on head kinematics. The outer helmet shell stiffness (Young's modulus, E) was varied between 0.2 and 1.0 GPa and the buckling column instantaneous shear modulus (G_0) was varied between 0.01 and 0.1 GPa. E and G_0 in the developed model are 0.55 and 0.038 GPa, respectively. A full factorial design, with 5 equally distributed levels of each stiffness parameter between the defined ranges was used to develop the simulation matrix (25 total simulations). The full sampling space is shown in the Supplementary Materials. The pendulum impact to the back of the helmet at 6.1 m/s was simulated for each sample point in the parametric space. This impact condition was chosen as it eliminated the influence of a deformable impactor and effectively isolated the effect of the outer shell and buckling layer. To assess the sensitivity of the head kinematics on helmet stiffness, surface plots for peak linear acceleration and peak angular velocity were constructed.

RESULTS

Material Characterization and Calibration

The calibrated quasi-static (10^{-1} 1/s) and intermediate rate (10^0) foam responses for the green, black, and yellow polyurethane foams are shown in Fig. 5. In addition, component-level simulation results, compared to experimental data, for the outer shell and buckling columns are shown in Fig. 6. In the final material model, the outer shell had a Young's modulus of 0.55 GPa and a Poisson's ratio of 0.4. Relative to other helmet models, the stiffness of the VZ1 outer shell was an order of magnitude softer. For instance, the outer shells of the 2016 Xenith X2E and 2016 Schutt Air XP Pro football helmets had Young's moduli of 2.45 and 1.84 GPa, respectively.^{2,3} The buckling column short- (G_0) and long-term (G_∞) shear moduli were 0.038 and 0.0105 GPa, respectively, with a time constant (β) of 0.001 1/ms. To prevent instabilities due to point loads at the interface between the buckling columns and the column shells, the shell elements immediately connected to the buckling beams (as shown in Fig. 3) were reinforced ($G_0 = 0.28$; $G_\infty = 0.105$ GPa). This was not found to influence the overall model response. Comprehensive material calibration and component-level validation results are included in the Supplementary Material.

Validation and Verification

A total of 62 impact simulations were run to verify the response and stability of the VZ1 model. All simulations were stable and completed normally, with the exception of the 9.3 m/s LI impact to the "F" location,

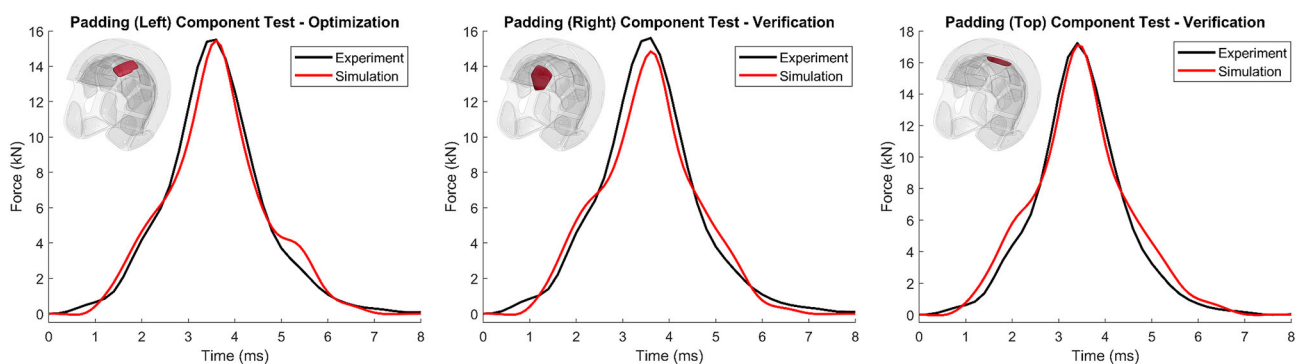


FIGURE 5. Component test results for three of the padding bonnet components. The left padding component test (left panel) was used to calibrate the short-term viscoelastic parameters of the padding foam material. The right padding (center panel) and top padding (right panel) simulations were used to verify the calibrated material properties.

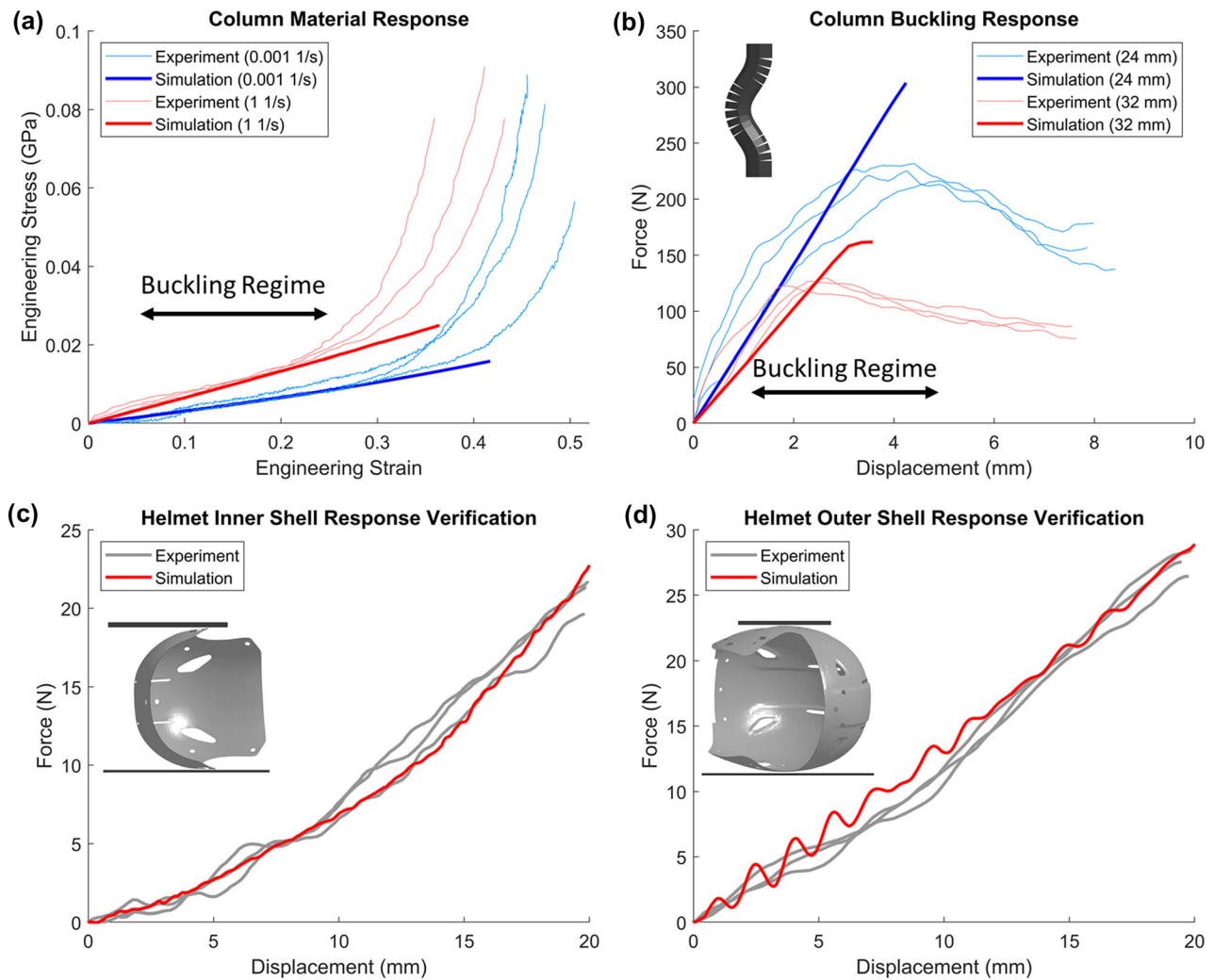


FIGURE 6. Component response for the columns, inner shell, and outer shell. (a) Column material response at strain rates of 0.001 and 1 1/s. The linear viscoelastic material was tuned to match the material response between 0 and 30% strain, which encapsulated the buckling regime. (b) Column buckling response verification response. Experiments were conducted with two different length column specimens (24 and 32 mm). (c) Inner shell component verification results. (d) Outer shell component verification results.

which error-terminated (41 ms) due to a non-physical interaction between the facemask and the VN foam located between the impact surface and the impactor ram. Of these simulations, 54 were used to validate the VZ1 model response. Overall, the model responses demonstrated similarity to the corresponding experimental data with overall CORA scores ranging from 0.81 to 0.90 for all validation cases, with the highest scores observed in the DI-H simulations.

The resultant head linear acceleration and load cell force for the NOCSAE 4.9 m/s impact to the top of the helmet is shown in Fig. 7. The overall CORA score for this specific case was 0.84 (Table 2). The effect of column buckling can be observed in the experimental force-time history for this impact case. Prior to buckling, the load cell force increases at a constant rate

as the effective stiffness of the helmet is engaged. At the time that buckling commences (3 ms), the force decreases slightly before increasing again as the buckling layer compacts (3–10 ms). Finally, the load returns to zero as the buckling layer unloads and the helmet rebounds (10–30 ms). CORA scores for all NOCSAE and HIII drop cases are included in the Supplementary Material and the mean CORA scores for all drop impacts ranged from 0.76 (HIII 2.9 m/s “top” impact) to 0.95 (HIII 2.9 m/s “side” impact), with a mean of 0.89 ± 0.04 . The mean percent difference between experimental and simulated peak resultant linear acceleration for the HIII and NOCSAE drop impacts was $11.9 \pm 9.2\%$.

Results from the 7.4 m/s oblique linear impact (location “D”) are shown in Fig. 8. For this specific case,

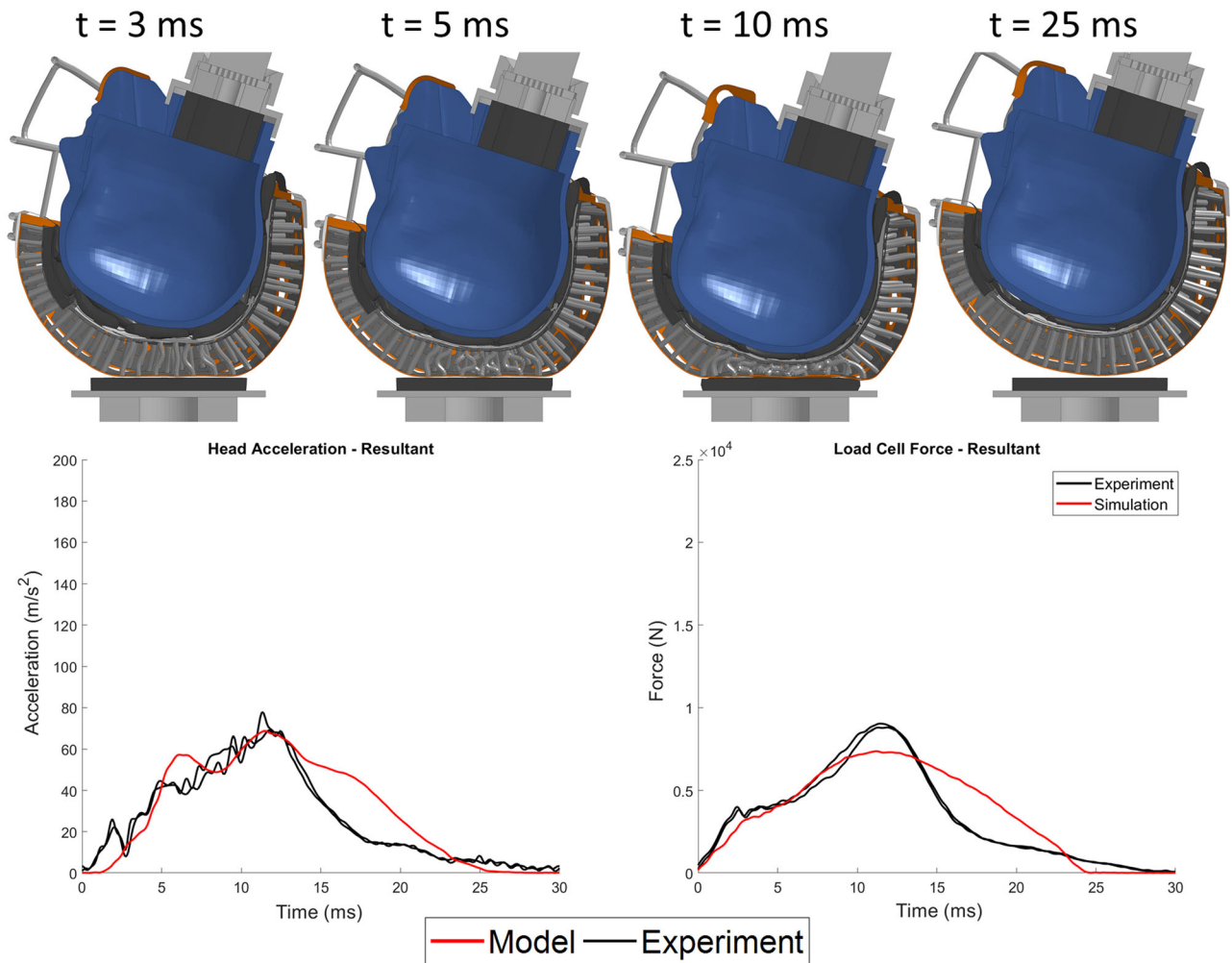


FIGURE 7. VZ1 validation response in the NOCSAE drop test (“top” impact location, 4.9 m/s). (Top) mid-sagittal cross-section demonstrating the time progression of the buckling response. (Bottom) resultant head acceleration (left) and resultant load cell force (right). Model response is shown in red.

TABLE 2. CORA scores for the 4.9 m/s HIII and NOCSAE drop impact cases.

Headform	Metric	Rear	Front	Side	Top
HIII	Hammer acceleration	0.84	0.90	0.92	0.87
	Res. head linear acceleration	0.80	0.93	0.90	0.88
	Res. load cell force	0.95	0.98	0.97	0.94
	Mean: overall	0.86	0.94	0.93	0.90
NOCSAE	Hammer acceleration	0.88	0.86	0.88	0.82
	Res. head linear acceleration	0.79	0.91	0.86	0.82
	Res. load cell force	0.92	0.95	0.89	0.87
	Mean: overall	0.86	0.91	0.88	0.84

the overall CORA score was 0.94 (Table 3). Overall, CORA scores for the LI cases ranged from 0.66 (9.3 m/s “AP” location) to 0.94 (7.4 m/s “D” location), with a mean of 0.86 ± 0.07 . For all impact velocities, CORA scores were best for the “D” and

“UT” impact locations and poorest for the “AP” impact location. CORA scores for all impact locations and velocities are included in the Supplementary Material. The mean percent difference between experimental and simulated peak resultant linear accelera-

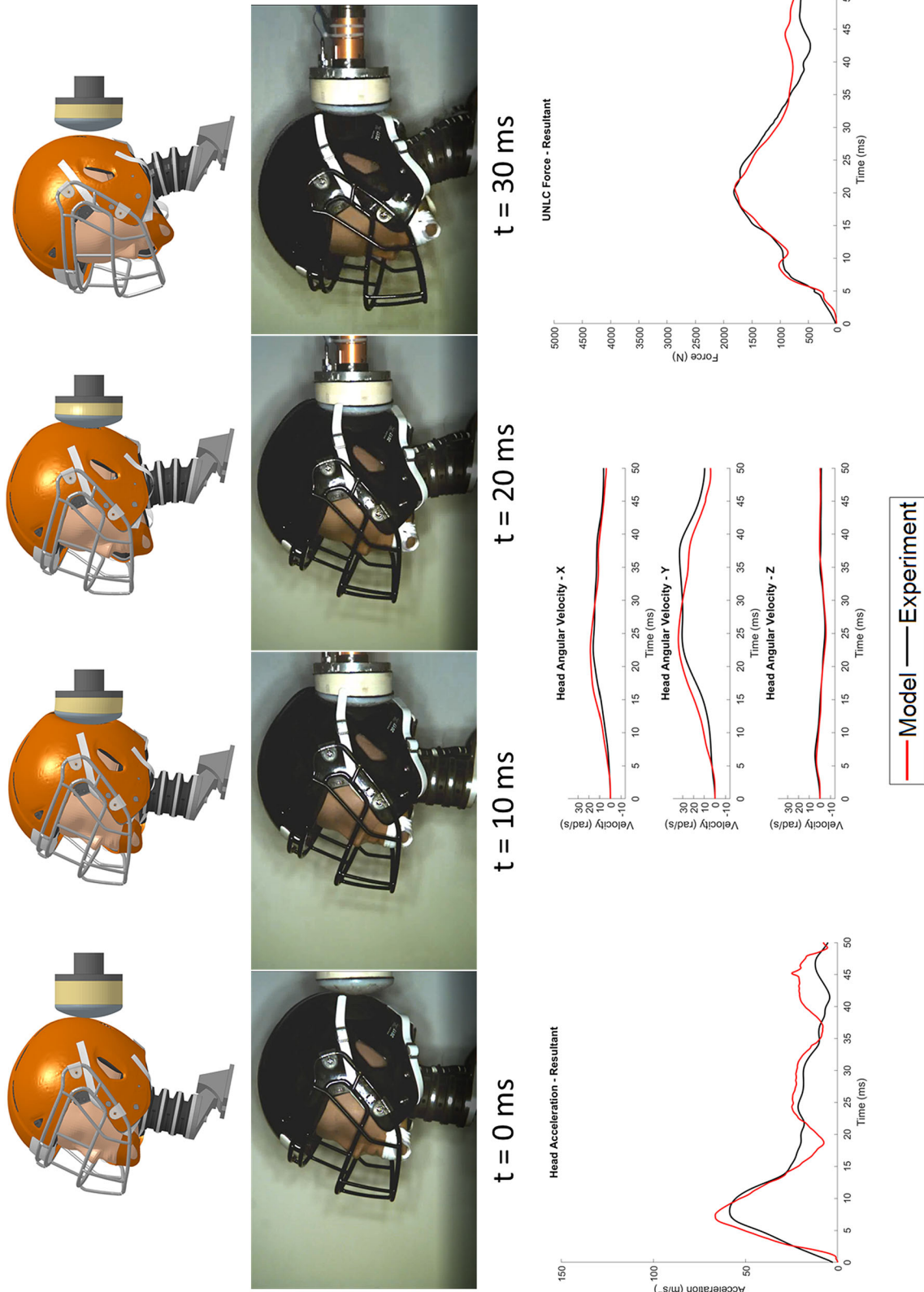


FIGURE 8. VZ1 model validation response in the linear impact test (“D” impact location, 7.4 m/s). Top: simulation progression from 0 to 30 ms compared to test videos. Bottom: HIII head resultant acceleration (left), angular velocity (middle), and resultant UNLC force (right). Simulation results are shown in red and experimental data is shown in black.

TABLE 3. CORA scores for the 7.4 m/s linear impact cases.

Metric	Rear R	Frontal AP	Lateral		Oblique		
			C	UT	A	B	D
Ram acceleration	0.93	0.73	0.89	0.92	0.88	0.98	0.96
Ram force	0.91	0.69	0.88	0.93	0.86	0.93	0.92
Res. head linear acceleration	0.82	0.66	0.92	0.95	0.87	0.92	0.95
Head angular velocity	0.83	0.69	0.74	0.81	0.65	0.82	0.90
Res. UNLC force	0.93	0.64	0.94	0.95	0.82	0.85	0.98
Mean: overall	0.89	0.68	0.87	0.91	0.81	0.90	0.94

tion and angular velocity for these cases were $11.1 \pm 9.1\%$ and $12.7 \pm 8.5\%$, respectively. For the LI condition, the “F” impact location was not included in the model validation process.

Results from the 4.6 m/s pendulum impact are shown in Fig. 9. For the PI cases, experimental video documentation was not available. For this impact, the overall CORA score was 0.83 (Table 4). While the simulated x and y angular velocity time-histories matched the experimental data, the z angular velocity response was over-predicted in the simulation (Fig. 9). This may have been due to a slight mismatch between the pendulum positioning in the simulation compared to what was reported in the experimental protocol.^{10,11} In general, CORA scores for the PI cases ranged from 0.68 (3.0 m/s “FrontBoss” impact) to 0.91 (3.0 m/s “Side” impact), with a mean of 0.81 ± 0.07 . Scores were poorest in the “FrontBoss” impact location and greatest in the “Side” impact location. CORA scores for all PI impacts are included in the Supplementary Material. The mean percent difference between experimental and simulated peak resultant linear acceleration and angular velocity for these cases were $27.6 \pm 14.1\%$ and $45.3 \pm 64.2\%$, respectively. However, these were significantly influenced by the “FrontBoss” cases, which also had the poorest CORA scores (Table 4). Neglecting these impact cases, these means were $21.5 \pm 8.9\%$ and $9.0 \pm 4.6\%$, respectively.

Parametric Study on Helmet Stiffness

To investigate the effect of outer shell and column stiffness on the head kinematics, 25 simulations were run in the 6.1 m/s “back” pendulum impact with varying outer shell ($E = 0.2\text{--}1.0$ GPa) and column stiffnesses ($G_0 = 0.01\text{--}0.1$ GPa). In this range of material parameters, the maximum resultant head linear acceleration was found to be highly sensitive, with values ranging from 80 to 220 G’s. It is evident that there is a tradeoff between shell and column stiffness with optimal values (with respect to minimizing head acceleration) of $E = 0.5\text{--}0.7$ GPa and

$G_0 = 0.06\text{--}0.07$ GPa (Fig. 10a). Furthermore, increasing the instantaneous shear modulus of the columns from 0.01 to 0.055 GPa, while maintaining the outer shell stiffness constant, was found to decrease the maximum head acceleration and prevent the compaction of the buckling layer (Fig. 10c). However, a further increase in column stiffness from 0.055 to 0.1 GPa resulted in a slight increase in peak head acceleration. Increasing outer shell stiffness, while maintaining the column instantaneous shear stiffness constant, resulted in a relatively linear reduction in peak head acceleration. However, for the range in material parameters investigated, increasing the outer shell stiffness to 1 GPa was not enough to prevent buckling layer compaction in this impact case (Fig. 10). Maximum resultant head angular velocity was less sensitive to helmet stiffness, with values ranging from 37 to 40 rad/s (Fig. 10b).

DISCUSSION

In this study, a FE model of the VZ1 helmet was developed using a comprehensive bottom-up approach and extensively validated using four different impact test methodologies that are commonly used to assess football helmet performance (Fig. 1). These impact tests included a wide range of impact velocities (2.9–9.3 m/s), impact locations (front, side, rear, top, oblique, and facemask), impactor types (rigid and deformable), and headforms (HIII and NOCSAE). Overall, the model demonstrated a good correlation to the laboratory test data with an overall CORA score of 0.86 ± 0.07 (range 0.66–0.95) for all 54 cases.

The helmet model was developed using a bottom-up framework where material parameters were iteratively tuned to match material test data. Component-level validation was essential to verify the response of the constitutive models and ensure that the geometries of the VZ1 parts were accurately represented in the model. In general, the component-level validation responses demonstrated excellent fidelity compared to the experimental data over the relevant loading ranges

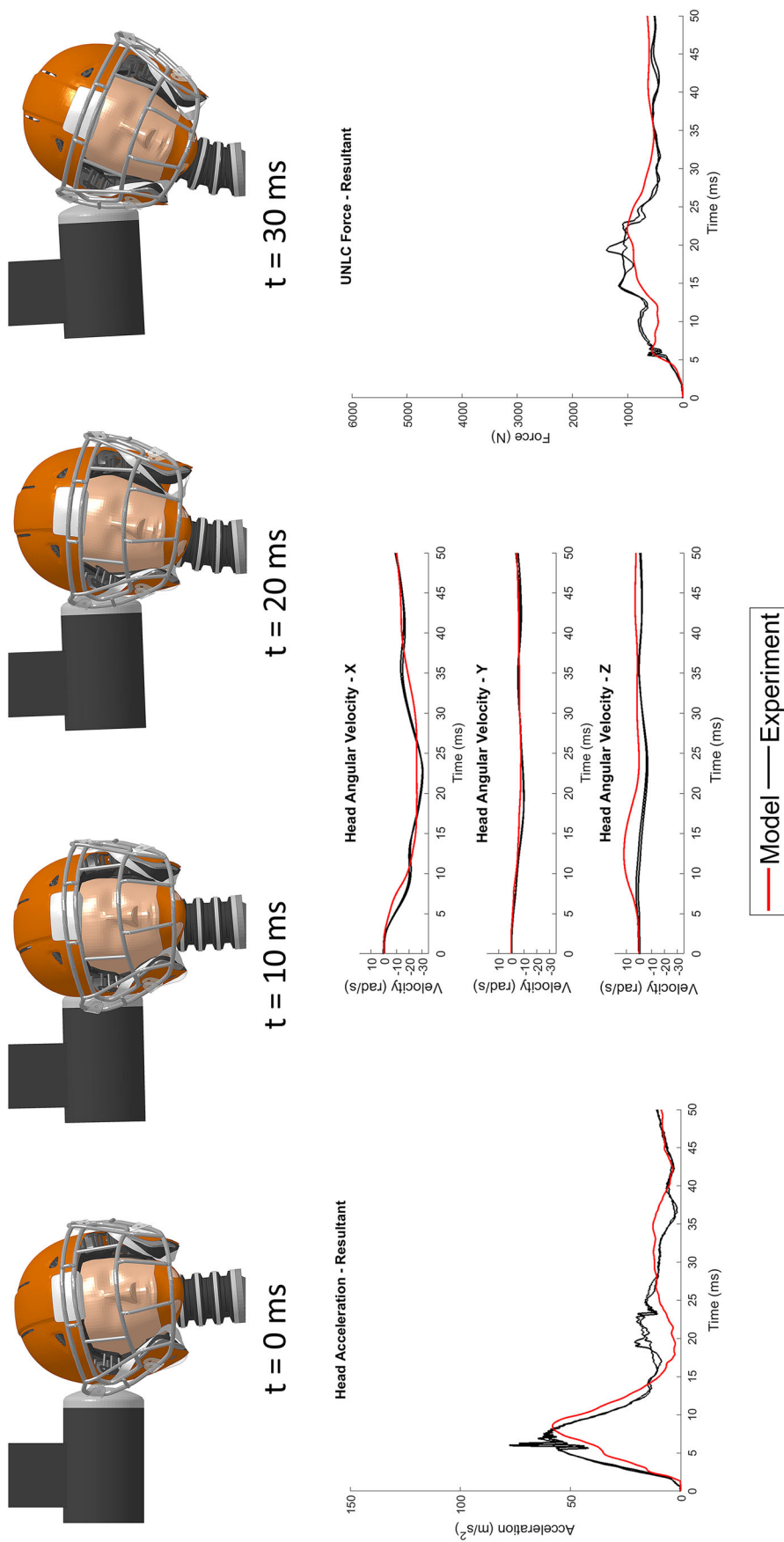


FIGURE 9. VZ1 model validation response in the pendulum impact test (“Side” impact location, 4.6 m/s). Top: simulation progression from 0 to 30 ms. Videos of the experimental tests were not available. Bottom: Hill head resultant acceleration (left), angular velocity (middle), and resultant UNLC force (right). Simulation results are shown in red and repeated experimental tests are shown in black.

and rates. These accurate responses translated to the full-scale helmet validation impact simulations.

Given the unique deformable nature of the VZ1 helmet, it was important to obtain an accurate representation of the deformable outer shell and buckling columns. In the component-level validation simulation, the inner and outer shell response accurately

TABLE 4. CORA scores for the 4.6 m/s pendulum impact cases.

Metric	Rear	FrontBoss	Side
Pendulum acceleration	0.88	0.92	0.80
Res. head linear acceleration	0.86	0.62	0.83
Head angular velocity	0.74	0.62	0.81
Res. UNLC force	0.87	0.80	0.88
Mean: overall	0.84	0.74	0.83

matched the experimental data (Fig. 6). Modeling and implementing the columns posed a greater challenge due to material nonlinearities and the fixed-fixed boundary conditions at either end of the column. For the columns, a linear viscoelastic material model with a single time constant was utilized, as it was the only viscoelastic material option for 1D elements in LS-DYNA. While this material enabled rate dependence, the nonlinearity of the material at high deformation was not captured (Fig. 6a). However, the material response over the first 20–30% strain matched the experimental data. This was acceptable as buckling occurred at approximately 10–15% strain (Fig. 6b). Furthermore, because more time constants were not available, it is likely that the unloading behavior of the buckling columns was less accurate, which was evident in the load cell force response in the 4.9 m/s DI-N impact to the top of the helmet (Fig. 7). Modeling the buckling columns with 3D elements was not feasible as

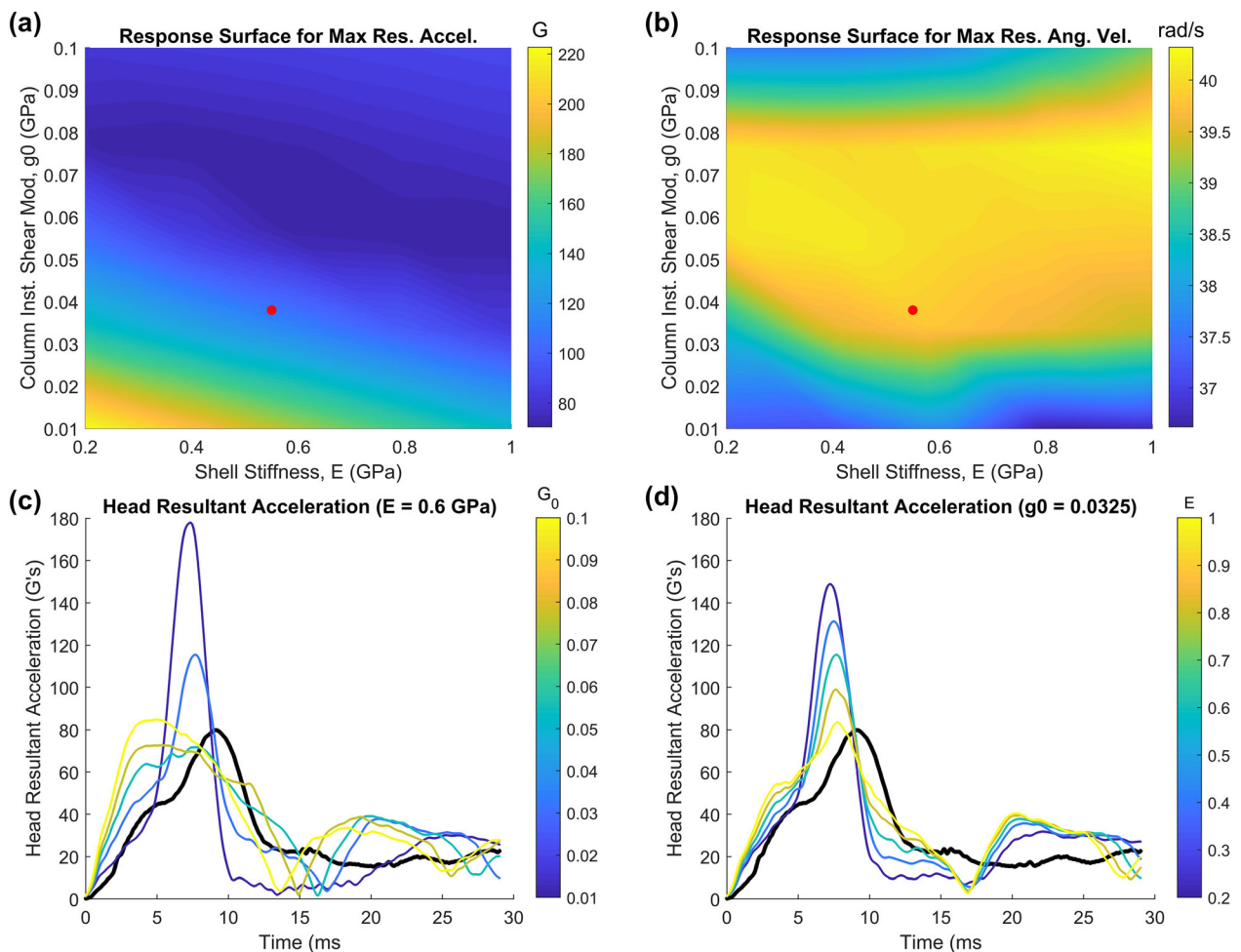


FIGURE 10. Results from the parametric study on helmet stiffness. (a) Response surface for maximum resultant acceleration. (b) Response surface for maximum resultant angular velocity. The material parameters in the developed helmet model are indicated by red dots. (c) Head resultant acceleration time-histories as the column instantaneous shear modulus is increased. (d) Head resultant acceleration time-histories as the helmet shell stiffness is increased. For (c) and (d) the experimental data is shown in black..

a preliminary convergence study showed that to obtain an accurate buckling response each column would require over 12,000 elements (see Supplementary Material).

There were additional modeling simplifications that were required to develop an efficient model. The linear impactor model did not have a detachable VN foam pad, and as a result, the simulated “F” impact cases had the nylon impactor face pull on the facemask during unloading. This did not occur in the tests because the VN foam was able to detach from the impactor. Because of these substantial differences, the “F” impact location was not considered in the model validation process. The only other LI case where this occurred was the 9.3 m/s “AP” impact, however, the separation of the VN foam did not directly influence the head or helmet kinematics and was included in the CORA analysis. The second model simplification was not accounting for any neck bending prior to impact. In cases where the HIII H–N was positioned at a substantial angle, it was possible that the neck bent slightly under the weight of the headform and helmet, which was approximately 6.7 kg for the VZ1 and HIII. This would have resulted in an effective HIII H–N angle that was slightly larger than specified in the experimental protocol. In the PI “front” barehead impacts, it was suspected that the weight of the HIII head alone resulted in an additional 2° of neck bending.¹¹ In most cases, this slight discrepancy was not found to influence the model results. However, in the PI “front” helmeted impacts, this slight discrepancy influenced where the impactor contacted the facemask. Whether or not the impactor contacted the facemask had a large effect on the head kinematics and because the exact impact location could not be verified, the “front” pendulum impact cases were excluded from the validation assessment. However, all “front” pendulum impact simulations were stable.

Given the unique deformable characteristics of the VZ1 helmet, a parametric investigation was performed to investigate the effect of the helmet structural stiffness on head kinematics. This was performed solely to explore the helmet response sensitivity and robustness, and not as an optimization of the helmet design, as many other design variables, impact conditions, and loading environments would need to be considered. The results of this parametric study elucidated two primary observations. First, angular velocity was not sensitive to helmet stiffness. In all simulations, the maximum resultant head angular velocity only varied by 3 rad/s (37–40 rad/s, Fig. 10a). Conversely, maximum resultant head linear acceleration varied by 140 G’s (80–220 G’s, Fig. 10b). For all material parameter combinations, substantial buckling was observed even with the stiffest combination of material properties. It

is possible that the head angular velocity response is sensitive to helmet effective stiffness as helmet buckling is reduced or eliminated, and more simulations are required to determine whether this is a general finding or a characterization of this loading condition. This is an important avenue for future investigation as concussions are known to be predominantly caused by rotational head kinematics and not linear head kinematics.^{1,6,7,12,16,23}

Secondly, it was found that there was a nonlinear relationship between helmet stiffness and head linear acceleration. For a constant outer shell stiffness, the head acceleration decreased as the buckling layer stiffness increased from 0.01 to 0.055 GPa (Fig. 10c). Increasing the column stiffness increased the buckling force and reduced compaction of the buckling layer. However, increasing buckling column stiffness from 0.055 to 0.1 GPa resulted in a slight increase in peak head resultant acceleration. Although buckling compaction was insignificant in these cases, the reduction of helmet deformation and associated decrease in the contact time resulted in increased head kinematics (Fig. 10c). For a constant column stiffness, increasing outer shell stiffness resulted in decreased head acceleration. This relationship was relatively linear as modifying the outer shell stiffness did not influence the buckling characteristics of the columns (Fig. 10d). In summary, as the helmet stiffness increases, local deformations are decreased, and the loads are more evenly distributed over the helmet’s structure. However, helmet deformation appears to be beneficial and if the helmet is too stiff, helmet deformation is eliminated. Future investigations should be conducted to identify helmet characteristics that influence angular head kinematics as angular head motion is strongly related to mTBI risk.

There were several limitations in this study. Firstly, material test data were obtained over a range of strain rates, but higher strain rates may be experienced in severe real-world impacts. For instance, in the dynamic drop tests performed to characterize the high rate response of the padding components resulted in strain rates of approximately 100 1/s. However, in the 9.3 m/s “R” LI simulation, strain rates exceeded 200 1/s. Therefore, it is possible that the material response at very high rates is not sufficiently captured. Nonetheless, these effects are likely minimal since these exceptionally high strain rates only occur in less than 1% of the duration of loading. In a preliminary sensitivity study on the effect of padding stiffness, increasing padding stiffness by a factor of 5 did not substantially influence model results in the 6.0 m/s DI-H back and 4.9 m/s DI-N top impacts. Secondly, foam prestresses, as a result of foam compression during fitting, were not included in the impact simulations. Simulations were

run with prestresses defined (through *INITIAL_FOAM_REFERENCE_GEOMETRY, in LS-DYNA) and did not affect model outputs substantially. Furthermore, the inclusion of prestress increased the likelihood of instabilities in the padding components. Prestress files are included in the available model package. Additionally, it is important to emphasize that the sensitivity study results were obtained from a single impact condition and further research is required to quantify the effect of helmet stiffness on head kinematics and the associated injury risk. The effect of additional parameters such as impactor-to-helmet friction, chinstrap fit and connectivity, helmet mass and inertia, and impact velocity and location should also be investigated. Finally, the helmet model developed in this study was validated for head linear acceleration and angular velocity and should be considered when interpreting helmet model responses and brain injury metrics, such as UBrIC⁶ and DAMAGE.⁷

The VZ1 model is one of four FE models of modern football helmets. Collectively, these models provide an *in silico* design platform for advanced helmet development and will be fundamental for understanding how novel helmet designs influence brain injury risk. These models are freely available for public use and can be downloaded at <http://biocore.com/resources>.

ELECTRONIC SUPPLEMENTARY MATERIAL

The online version of this article (<https://doi.org/10.1007/s10439-020-02472-6>) contains supplementary material, which is available to authorized users.

ACKNOWLEDGMENTS

The research presented in this paper was made possible by a Grant from Football Research, Inc. (FRI). The views expressed are solely those of the authors and do not represent those of FRI or any of their affiliates or funding sources. The authors would like to thank our collaborators in the “Engineering Roadmap: Numerical Crowdsourcing Project” for their support and feedback of this work (Teams from Wake Forest University, University of Waterloo, and KTH Royal Institute of Technology). The authors also acknowledge the Virginia Tech Helmet Lab and BioKinetics and Associates, Ltd. for generating the pendulum and linear impactor test data. Finally, the authors would like to thank Dr. Lee Gabler, Dr. Anne Bailey, and Dr. Wei Zeng for their feedback.

CONFLICT OF INTEREST

The authors declare no conflicts of interest.

REFERENCES

- ¹Alshareef, A., J. S. Giudice, J. Forman, R. S. Salzar, and M. B. Panzer. A novel method for quantifying human in situ whole brain deformation under rotational loading using sonomicrometry. *J. Neurotrauma* 35:780–789, 2018. <https://doi.org/10.1089/neu.2017.5362>.
- ²Bustamante, M. C., D. Bruneau, J. B. Barker, D. Gierczycka, M. A. Coralles, and D. S. Cronin. Component-level finite element model and validation for a modern American football helmet. *J. Dyn. Behav. Mater.* 2019. <https://doi.org/10.1007/s40870-019-00189-9>.
- ³Corrales, M. A., D. Gierczycka, J. B. Barker, D. Bruneau, M. C. Bustamante, and D. S. Cronin. Validation of a football helmet finite element model and quantification of impact energy distribution. *Ann. Biomed. Eng.* 48:1–12, 2019.
- ⁴Decker, W., A. Baker, X. Ye, P. Brown, J. Stitzel, and F. S. Gayzik. Development and multi-scale validation of a finite element football helmet model. *Ann. Biomed. Eng.* 2019. <https://doi.org/10.1007/s10439-019-02345-7>.
- ⁵Funk, J. R., J. Crandall, M. Wonnacott, and C. Withnall. NFL Linear Impactor Helmet Test Protocol. Charlottesville: Biomechanics Consulting Research, 2017.
- ⁶Gabler, L. F., J. R. Crandall, and M. B. Panzer. Development of a metric for predicting brain strain responses using head kinematics. *Ann. Biomed. Eng.* 46:972–985, 2018. <https://doi.org/10.1007/s10439-018-2015-9>.
- ⁷Gabler, L. F., J. R. Crandall, and M. B. Panzer. Development of a second-order system for rapid estimation of maximum brain strain. *Ann. Biomed. Eng.* 2019. <https://doi.org/10.1007/s10439-018-02179-9>.
- ⁸Gehre, C., H. Gades, and P. Wernicke. Objective rating of signals using test and simulation responses. In: 21st International Technical Conference on the Enhanced Safety of Vehicles, Stuttgart, Germany, 2009.
- ⁹Gessel, L. M., S. K. Fields, C. L. Collins, R. W. Dick, and R. D. Comstock. Concussions among United States high school and collegiate athletes. *Yearb. Sports Med.* 2009:19–20, 2009. [https://doi.org/10.1016/S0162-0908\(08\)79294-8](https://doi.org/10.1016/S0162-0908(08)79294-8).
- ¹⁰Giudice, J. S., and M. B. Panzer. Effect of initial positioning of the Hybrid III Head–Neck in frontal and oblique bare head impact. In: IRCOBI Conference Proceedings. Presented at the 2018 International Research Council on Biomechanics of Injury (IRCOBI), 2018.
- ¹¹Giudice, J. S., G. Park, K. Kong, A. Bailey, R. Kent, and M. B. Panzer. Development of open-source dummy and impactor models for the assessment of American football helmet finite element models. *Ann. Biomed. Eng.* 47:464–474, 2019. <https://doi.org/10.1007/s10439-018-02155-3>.
- ¹²Giudice, J. S., W. Zeng, T. Wu, A. Alshareef, D. F. Shedd, and M. B. Panzer. An analytical review of the numerical methods used for finite element modeling of traumatic brain injury. *Ann. Biomed. Eng.* 2018. <https://doi.org/10.1007/s10439-018-02161-5>.
- ¹³Hallquist, J. O. LS-DYNA Theory Manual, Version 3. Livermore: Livermore Softw. Technol. Corp., pp. 25–31, 2006.

- ¹⁴Hallquist, J. O. LS-DYNA Keyword User's Manual Version 970. Livermore: Livermore Softw. Technol. Corp., 2007.
- ¹⁵Hodgson, V. R. National Operating Committee on Standards for Athletic Equipment football helmet certification program. *Med. Sci. Sports* 7:225–232, 1975.
- ¹⁶Holbourn, A. H. S. Mechanics of head injuries. *Lancet* 242:438–441, 1943. [https://doi.org/10.1016/S0140-6736\(00\)87453-X](https://doi.org/10.1016/S0140-6736(00)87453-X).
- ¹⁷Joodaki, H., A. Bailey, D. Lessley, J. Funk, C. Sherwood, and J. Crandall. Relative motion between the helmet and head in football impact test. *J. Biomech. Eng.* 2019. <https://doi.org/10.1115/1.4043038>.
- ¹⁸Langlois, J. A., W. Rutland-Brown, and M. M. Wald. The epidemiology and impact of traumatic brain injury: a brief overview. *J. Head Trauma Rehabil.* 21:375–378, 2006. <https://doi.org/10.1097/00001199-200609000-00001>.
- ¹⁹Levy, M. L., B. M. Ozgur, C. Berry, H. E. Aryan, and M. L. J. Apuzzo. Birth and evolution of the football helmet. *Neurosurgery* 55:656–662, 2004. <https://doi.org/10.1227/01.NEU.0000134599.01917.AA>.
- ²⁰National Football League (NFL). 2017 Helmet Laboratory Testing Performance Results. National Football League (NFL), 2017.
- ²¹Panzer, M. B., J. S. Giudice, A. Caudillo, S. Mukherjee, K. Kong, D. S. Cronin, J. Barker, D. Gierczycka, M. Bustamante, D. Bruneau, M. Corrales, P. Halldin, M. Fahlstedt, M. Arnesen, E. Jungstedt, F. S. Gayzik, J. D. Stitzel, W. Decker, A. M. Baker, X. Ye, and P. Brown. Numerical crowdsourcing of NFL football helmets. *J. Neurotrauma* 35:A148–A148, 2018.
- ²²SAE. User's Manual for the 50th Percentile Male Hybrid III Test Dummy. Warrendale: SAE, 1998.
- ²³Takhounts, E. G., M. J. Craig, K. Moorhouse, J. McFadden, and V. Hasija. Development of brain injury criteria (Br IC). *Stapp Car Crash J.* 57:243–266, 2013.
- ²⁴Vicis, Inc. Zero1. Vicis, 2019. <https://vicis.com/products/zero1>. Accessed 3.12.2019.

Publisher's Note Springer Nature remains neutral with regard to jurisdictional claims in published maps and institutional affiliations.